Original research

A fusion-based deep-learning algorithm predicts PDAC metastasis based on primary tumour CT images: a multinational study

Nannan Xue,[1] Sergio Sabroso-Lasa,[1] Xavier Merino,[2] Maria Munzo-Beltran,[3] Megan Schuurmans ,[4] Maria Olano,[1] Lidia Estudillo ,[5] Maria Jesús Ledesma-Carbayo,[6,7] Junqi Liu,[8] Ruitai Fan,[8] John J Hermans,[9] Casper van Eijck,[10] Nuria Malats ,[1] PanGenEU Centres and Investigators

► Additional supplemental material is published online only. To view, please visit the journal online (https://doi.org/10.1136/gutjnl-2024-334237).

For numbered affiliations see end of article.

Correspondence to
Dr Nuria Malats; nuria@cnio.es

NX and SS-L contributed equally.

Received 18 November 2024
Accepted 4 June 2025
Published Online First 19 June 2025

To cite: Xue N, Sabroso-Lasa S, Merino X, *et al*. *Gut* 2025;**74**:2024–2034.

ABSTRACT

Background Diagnosing the presence of metastasis of pancreatic cancer is pivotal for patient management and treatment, with contrast-enhanced CT scans (CECT) as the cornerstone of diagnostic evaluation. However, this diagnostic modality requires a multifaceted approach.

Objective To develop a convolutional neural network (CNN)-based model (PMPD, Pancreatic cancer Metastasis Prediction Deep-learning algorithm) to predict the presence of metastases based on CECT images of the primary tumour.

Design CECT images in the portal venous phase of 335 patients with pancreatic ductal adenocarcinoma (PDAC) from the PanGenEU study and The First Affiliated Hospital of Zhengzhou University (ZZU) were randomly divided into training and internal validation sets by applying fivefold cross-validation. Two independent external validation datasets of 143 patients from the Radboud University Medical Center (RUMC), included in the PANCAIM study (RUMC-PANCAIM) and 183 patients from the PREOPANC trial of the Dutch Pancreatic Cancer Group (PREOPANC-DPCG) were used to evaluate the results.

Results The area under the receiver operating characteristic curve (AUROC) for the internally tested model was 0.895 (0.853–0.937) and 0.779 (0.741–0.817) in the PanGenEU and ZZU sets, respectively. In the external validation sets, the mean AUROC was 0.806 (0.787–0.826) for the RUMC-PANCAIM and 0.761 (0.717–0.804) for the PREOPANC-DPCG. When stratified by the different metastasis sites, the PMPD model achieved the average AUROC between 0.901–0.927 in PanGenEU, 0.782–0.807 in ZZU and 0.761–0.820 in PREOPANC-DPCG sets. A PMPD-derived Metastasis Risk Score (MRS) (HR: 2.77, 95% CI 1.99 to 3.86, p=1.59e−09) outperformed the Resectability status from the National Comprehensive Cancer Network guideline and the CA19-9 biomarker in predicting overall survival. Meanwhile, the MRS could potentially predict developed metastasis (AUROC: 0.716 for within 3 months, 0.645 for within 6 months).

Conclusion This study represents a pioneering utilisation of a high-performance deep-learning model to predict extrapancreatic organ metastasis in patients with PDAC.

WHAT IS ALREADY KNOWN ON THIS TOPIC

⇒ Early and accurate detection of metastasis from pancreatic ductal adenocarcinoma remains a critical challenge with conventional methods often resulting in delayed identification.

WHAT THIS STUDY ADDS

⇒ We developed a deep-learning model that accurately predicts the presence of distant metastases in patients diagnosed with pancreatic ductal adenocarcinoma using contrast-enhanced CT images of the primary tumour.

HOW THIS STUDY MIGHT AFFECT RESEARCH, PRACTICE OR POLICY

⇒ This deep learning model holds promise for assisting surgeons and clinicians in the detection of metastases, potentially refining surgical planning and improving outcomes for patients with pancreatic cancer by enabling timely intervention.

INTRODUCTION

The detection of metastasis in pancreatic ductal adenocarcinoma (PDAC) is a crucial factor in managing and treating patients suffering from this disease. Regrettably, the majority of patients (52%) are diagnosed with metastatic disease at the time of diagnosis, rendering surgical resection unfeasible (https://seer.cancer.gov/statfacts/html/pancreas.html). The prognosis for those patients is extremely poor with a mere 2% 5-year survival rate.[1 2]

Despite advancements in diagnostic modalities, accurately ascertaining the metastatic status of PDAC remains a challenge. Common imaging modalities such as CT scans and MRIs have limitations in sensitivity and specificity. While they can detect extensive metastases, they may fail to identify smaller or less conspicuous lesions, particularly in organs with dense tissue or lower imaging resolution contrast.[3 4] Positron emission tomography (PET)/CT effectively identifies distant metastatic sites, particularly those that are metabolically active, even when they are not visible on traditional

anatomical imaging techniques. However, PET/CT has limitations in detecting very small lesions, especially in regions like the liver, where distinguishing pathological findings from background activity can be difficult.[5] Furthermore, it is not recommended as a standard examination due to its high economic cost and the frequent occurrence of false positive results.[6] Moreover, once patients present with radiographic signs of metastatic disease, the following diagnostic process relies heavily on a combination of radiological imaging, clinical tools and biomarkers (ie, Carbohydrate Antigen 19-9 (CA19-9)) and a final biopsy with pathological assessment. This diagnostic process is characterised by being labour-intensive with a significant financial cost.[7] Therefore, a pressing need exists to develop novel, non-invasive and inexpensive tools to guide clinical decision-making for metastasis in patients with PDAC.

A contrast-enhanced CT scan (CECT) is currently the primary diagnostic test for pancreatic cancer diagnosis in most patients. CECT scans usually assess the tumour's size, location, density and blood supply. It can also determine the tumours' local invasion and assess their resectability.[8]

Advances in deep learning (DL), specifically convolutional neural networks (CNN), have exhibited robust and scalable performance in medical imaging analyses, outperforming other machine learning algorithms and expecting to revolutionise the current medical practice.[9] In recent years, there has been a significant increase in DL techniques applied to CT images in patients with PDAC, achieving remarkable performance in the diagnosis[10–12] and the prognosis fields.[13–16] Regarding PDAC staging, DL techniques for lymph node metastasis prediction have been proposed.[17–20] To the best of our knowledge, only three machine-learning models based on CECT radiomics for predicting occult liver and peritoneal metastases have been published.[21–23] However, no previous and robust DL algorithm comprehensively supports distant organ metastasis prediction, except for liver and peritoneal metastasis.

In this study, we hypothesised that radiological features of the primary tumour, which may not be visible to human expert eyes but can be identified by DL algorithms, are associated with the presence of metastasis. Here, we report on the Pancreatic tumour Metastasis Prediction Deep-learning (PMPD) algorithm, a DL-based fusion model designed to predict the presence of distant metastasis from CECT images of primary PDAC tumour at the diagnosis time. The ultimate goal of PMPD is to serve as an auxiliary tool for radiologists in assessing patients with metastatic disease, aiding in the diagnostic process and informing treatment planning.

METHODS

Patient sets

In this international multicentre study, 661 patients with PDAC from studies in Spain, China and the Netherlands were considered, including ZZU (The First Affiliated Hospital of Zhengzhou University), PanGenEU, RUMC-PANCAIM (Radboud University Medical Center (RUMC), included in the PANCAIM study) and PREOPANC-DPCG (the PREOPANC trial of the Dutch Pancreatic Cancer Group) sets. Characteristics of the studies and the inclusion and exclusion criteria are in online supplemental figure 1A and online supplemental methods.

Notably, the RUMC-PANCAIM set from the Netherlands exclusively enrolled patients who only had liver metastasis. Furthermore, the PanGenEU, RUMC-PANCAIM and PREOPANC-DPCG sets provided information on overall survival, which was used to evaluate the model's prognostic capabilities. The PanGenEU and PREOPANC-DPCG sets contained information on metastasis development, allowing for evaluating the models' capability of developing metastasis prediction.

Image acquisition and annotation

We extracted the CT images from the picture archiving and communication system in hospital and took several steps to uniform them into the same format. After that, each slice image in the study underwent automatic segmentation, delineating the pancreas and the tumour regions using nnU-Net,[24] with subsequent manual checking using 3D slicer software (V.4.11.2) by trained students. Due to the intricate anatomical structures surrounding the pancreas and the inherent challenges in tumour delineation, the segmented tumour images and their corresponding masks were further scrutinised by diagnostic radiologists or abdominal oncologists with over 20 years of experience to achieve consensus. This multistep review process ensured that all segmentation results were consistent with clinical standards. In contrast, no corrections were made to the pancreas segmentations because of the strong performance of nnU-Net in this task. A detailed description of image acquisition and annotation is provided in online supplemental methods.

Image pre-processing

For patients who underwent both 64-slice and 128-slice spiral CT scans, only the 128-slice CT data were used due to superior resolution. Slice thickness was standardised to 2 mm for images and labels, and then the window width and level were adjusted to 250 and 75 Hounsfield units, respectively. Label noise was reduced via erosion and dilation, while pancreas and tumour boundaries were expanded to preserve margin features. To improve performance, images with the top four largest tumour areas were selected and cropped to the pancreas region using bounding boxes. Then, rotation-based data augmentation generated 24 patches per patient. The image and segmentation mask were combined into a dual-channel input before model training. More details of image pre-processing can be found in online supplemental methods.

Model construction, training and evaluation

In this study, we present a fusion DL model named PMPD (Pancreatic tumour Metastasis Prediction Deep learning-based algorithm). The model's structure consisted of three modules: FeatureExtractor, Fusion and Classifier, which integrates the different depth features derived from image and mask data. The model structure is presented in online supplemental figure 1B and online supplemental methods. We randomly divided the PanGenEU and ZZU sets into training and internal validation sets on five-fold cross-validation to develop and test the PMPD model considering the patient's level to assess impartially. At the slice level, the prediction probability for metastasis was obtained from the model's output. Youden Index (sensitivity + specificity – 1), to set-up the best threshold in area under the receiver operating characteristic curve (AUROC), was used to dichotomise the probability to classify the presence of metastasis in the internal test set. Similarly, at the patient level, based on the proportion of predictive slice-level metastasis generated from the CNN model, patients were classified as presence/absence of metastases by using the threshold that maximises the Youden Index on the internal test set. The model training and evaluation process are described in online supplemental methods.

Statistics analysis

After model training, we evaluated performance on internal and external validation sets using accuracy, sensitivity, specificity, F1-score, AUROC and area under the precision recall curve (AUPRC). Log-rank tests were used to assess prognosis differences between groups, and Kaplan-Meier curves generated survival plots. Univariable and multivariable Cox regression, adjusted for age, sex and data centre, estimated HRs with 95% CIs. We used the Grad-CAM technique to highlight the key regions relevant to metastasis.[25] More details of statistics methods can be found in online supplemental methods.

Patient and public involvement statement

Patients were not involved in this research.

RESULTS

Study design and characteristics of the cohorts

The implementation of this study encompassed four steps, as depicted in figure 1A. First, portal venous phase CECT images were procured and annotated. Second, images with venous phases underwent preprocessing to generate a single set for each patient. Third, these patient-specific image sets were fed into the network, yielding a Metastasis Risk Score (MRS)-based prediction for each image. Fourth, the networks' performance was internally and externally assessed and compared.

The model was trained and internally tested through a five-fold cross-validation methodology, using 335 patients diagnosed with PDAC. Those patients provided a total of 1340 slice-level images from the PanGenEU and ZZU sets. Subsequent test procedures were conducted using 326 patients with PDAC, 1304 images aggregated from two distinct external validation

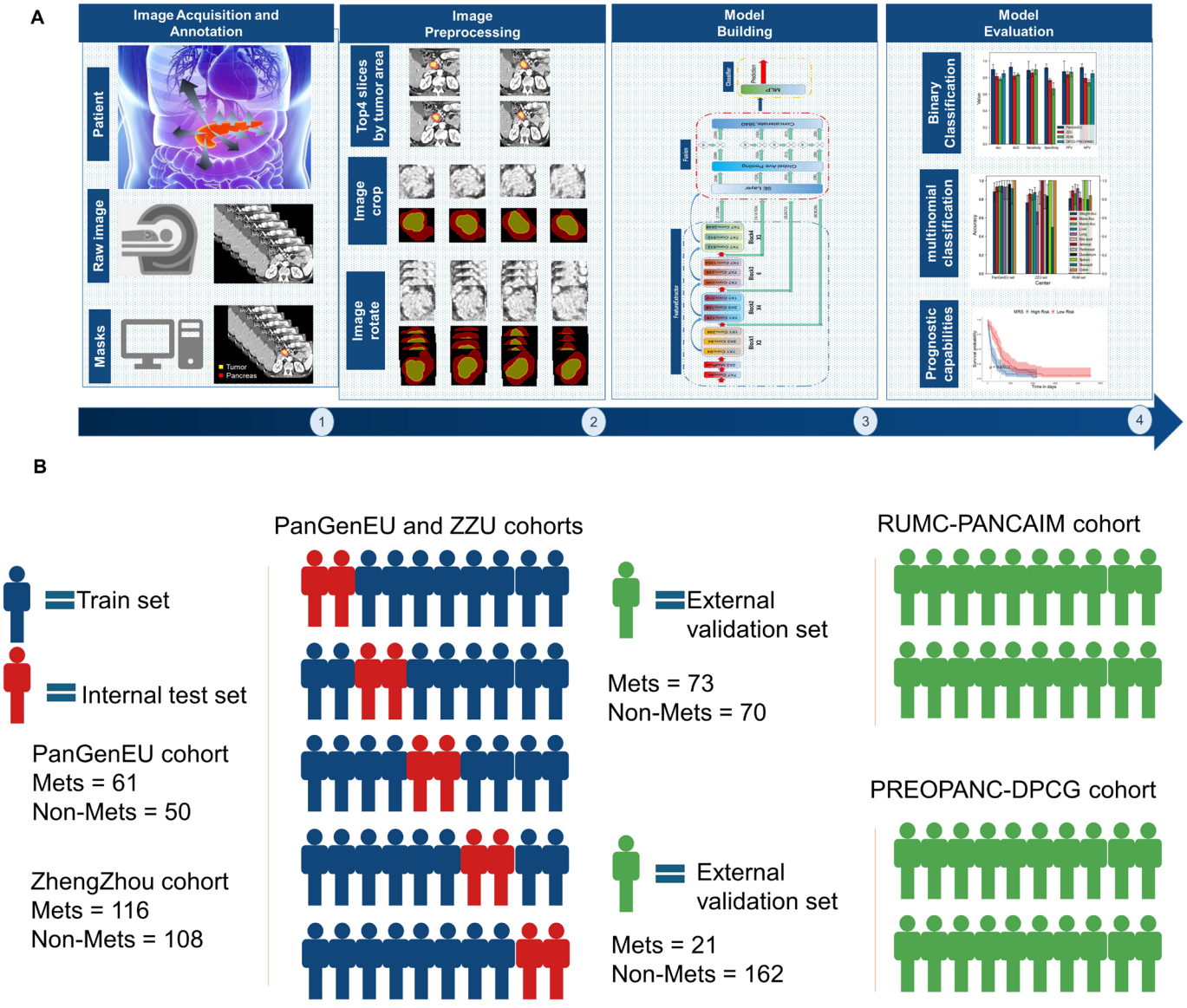

Figure 1 (A) Overview of the pipeline in this study. The pipeline consisted of image acquisition and annotation, image pre-processing, model building and model evaluation. (B) Patient sets: PanGenEU and ZZU sets were pooled and used for training the Pancreatic tumour Metastasis Prediction Deep learning-model and for the internal test to determine initial performance. RUMC-PANCAIM and PREOPANC-DPCG sets were used for the external validation. DPCG, Dutch Pancreatic Cancer Group; RUMC, Radboud University Medical Center; ZZU, The First Affiliated Hospital of Zhengzhou University.

sets: RUMC-PANCAIM and PREOPANC-DPCG (figure 1B). Comprehensive baseline characteristics of all the sets are presented in online supplemental table 1. The entire set's median (IQR) age was 66 (57–73), and 42.33% of the patients were women. The most common tumour location was the pancreatic head (58.55%). Overall, 208 (31.47%) patients had metastatic disease, including 178 (85.58%) with liver metastasis, 17 (8.17%) with lung metastasis, 21 (10.1%) with peritoneal metastasis and 4 (1.92%) with unknown metastatic location. Several tests were considered to determine the presence of metastases, which are shown in online supplemental table 2. Most cases of metastasis were identified by radiological images in PanGenEU and ZZU sets, while all patients in PREOPANC-DPCG set were identified by non-radiological tools. The information for the RUMC-PANCAIM set was missing. The median (IQR) follow-up was 400 (121–528) days, with 300 (73.71%) participants recorded as deceased.

Binary classification performance of the PMPD model to predict the presence/absence of metastases

First, our proposed DL model underwent evaluation at the CECT slice level. Subsequently, we implemented a fivefold cross-validation strategy to construct the PMPD model to discern the presence/absence of metastases at the slice level within the training set. Following the classification of each slice, the disease status at the patient level was inferred (figure 2A). The performance of the models was assessed across both internal and external validation datasets. The model's AUROC, accuracy, specificity, sensitivity, AUPRC and F1-score metrics at the slice level are displayed in online supplemental table 3.

On fivefold cross-validation, the AUROC for predicting the metastasis status at the patient level for the internally tested model was 0.895 (0.853–0.937) in the PanGenEU set and 0.779 (0.741–0.817) in the ZZU set (figure 2B and C, and online supplemental table 4). Figure 2D and E, and online supplemental figure 3 show the confusion matrices resulting from this internal test dataset. The rest of the performance metrics are displayed in figure 2J and K, and online supplemental table 4.

The prediction performance was then externally validated across two external datasets. In the RUMC-PANCAIM set, the PMPD model exhibited a mean AUROC value of 0.806 (0.787–0.826) at the patient level (figure 2F and online supplemental table 4); its confusion matrix is shown in figure 2G and online supplemental figure 3. In the PREOPANC-DPCG set, although the PMPD model achieved a mean AUROC value of 0.761 (0.717–0.804) (figure 2H and online supplemental table 4), its confusion matrix showed an imbalanced performance, especially for metastasis cases (figure 2I and online supplemental figure 3). The accuracy, AUPRC, specificity, sensitivity and F1-score metrics of the two external validation sets are shown in figure 2J and K, and online supplemental table 4. The performance on the 14 cases where <4 tumour-containing slices are shown in online supplemental table 5.

Furthermore, PMPD accurately predicted 65.8% (25/38) of metastases discovered through laparoscopy or during the surgical procedure that were not detected by radiographic imaging at diagnosis. In summary, these findings indicated the PMPD model's high potential ability to predict the presence/absence of distant metastasis in patients diagnosed with PDAC based on CECT tumour images.

Multinomial classification performance of the PMPD model when extended to the different metastasis sites

We subsequently proceeded to evaluate the PMPD model performance based on the different metastatic sites using the internal test sets (PanGenEU, ZZU) and external validation set (PREOPANC-DPCG) to ascertain whether its efficacy remained consistent across various metastatic sites (figure 3A). All metastatic cases from RUMC-PANCAIM set were found only in the liver, resulting in no multinomial classification performance. And the number of each fold for multinomial classification of metastasis sites in the internal test set is shown in the online supplemental table 6. The performance metrics at the slice level are displayed in online supplemental table 7. At the patient level, the PMPD model achieved a micro-average, macro-average and weighted-average AUROC between 0.901 and 0.927 in PanGenEU, 0.782 and 0.807 in ZZU and 0.761 and 0.820 in PREOPANC-DPCG sets, respectively (figure 3B, C and D, and online supplemental table 8). The average accuracy values are shown in figure 3E and online supplemental table 8.

The liver emerged as the most frequent site of metastasis, accounting for 178 (85.58%) patients across the three cohorts. Notably, for liver metastasis, the PMPD model exhibited high performance, with mean AUROC=0.894 (0.853–0.935) in the PanGenEU set, AUROC=0.776 (0.746–0.805) in the ZZU set and AUROC=0.703 (0.646–0.761) in the PREOPANC-DPCG set. Lung metastasis is a significant concern in clinics because a single abdominal CT image cannot detect it. In our datasets, 17 (8.71%) cases had lung metastasis. The PMPD model also exhibited high performance in detecting lung metastasis with mean AUROC=0.969 (0.946–0.993) in the PanGenEU set, AUROC=0.774 (0.652–0.895) in the ZZU set (figure 3B, C and D, and online supplemental table 8). Similar robust performance was observed for the peritoneal metastasis (figure 3B, C, D and E, and online supplemental table 8). Furthermore, none of the other potential confounding factors (ie, tumour size, location, age, sex and platform manufacturer) affected the model performance (online supplemental figure 4).

The MRS outperformed the Resectability status from the National Comprehensive Cancer Network guideline and CA19-9 biomarker in predicting overall survival and added prognostic value

In current clinical practice, PDAC oncologists and surgeons rely on the Resectability status based on CT scan assessment and CA19-9 biomarker levels to determine the appropriate management of patients, including surgical intervention or alternative treatments. Hence, we evaluated the prognostic prediction of the PMPD model at the time of diagnosis by comparing its performance against these established metrics (figure 4A). To achieve this, we initially collected the Resectability status data for 407 patients from the PanGenEU, RUMC-PANCAIM and PREOPANC-DPCG sets. These PanGenEU patients were used exclusively as internal test sets in each fold during cross-validation. Subsequently, CECT images of those patients were processed by the PMPD model to generate the MRS at the slice level, which was then averaged to get MRS at the patient level. The MRS values were dichotomised into high and low probability of metastasis using a cut-point determined by the maxstat test from the 'survminer' R package. For comparison with CA19-9 levels, data from 315 patients in the PanGenEU, RUMC-PANCAIM and PREOPANC-DPCG datasets were used. High and low CA19-9 categories were defined using a cut-point of 500 U/mL, the threshold used in the clinical

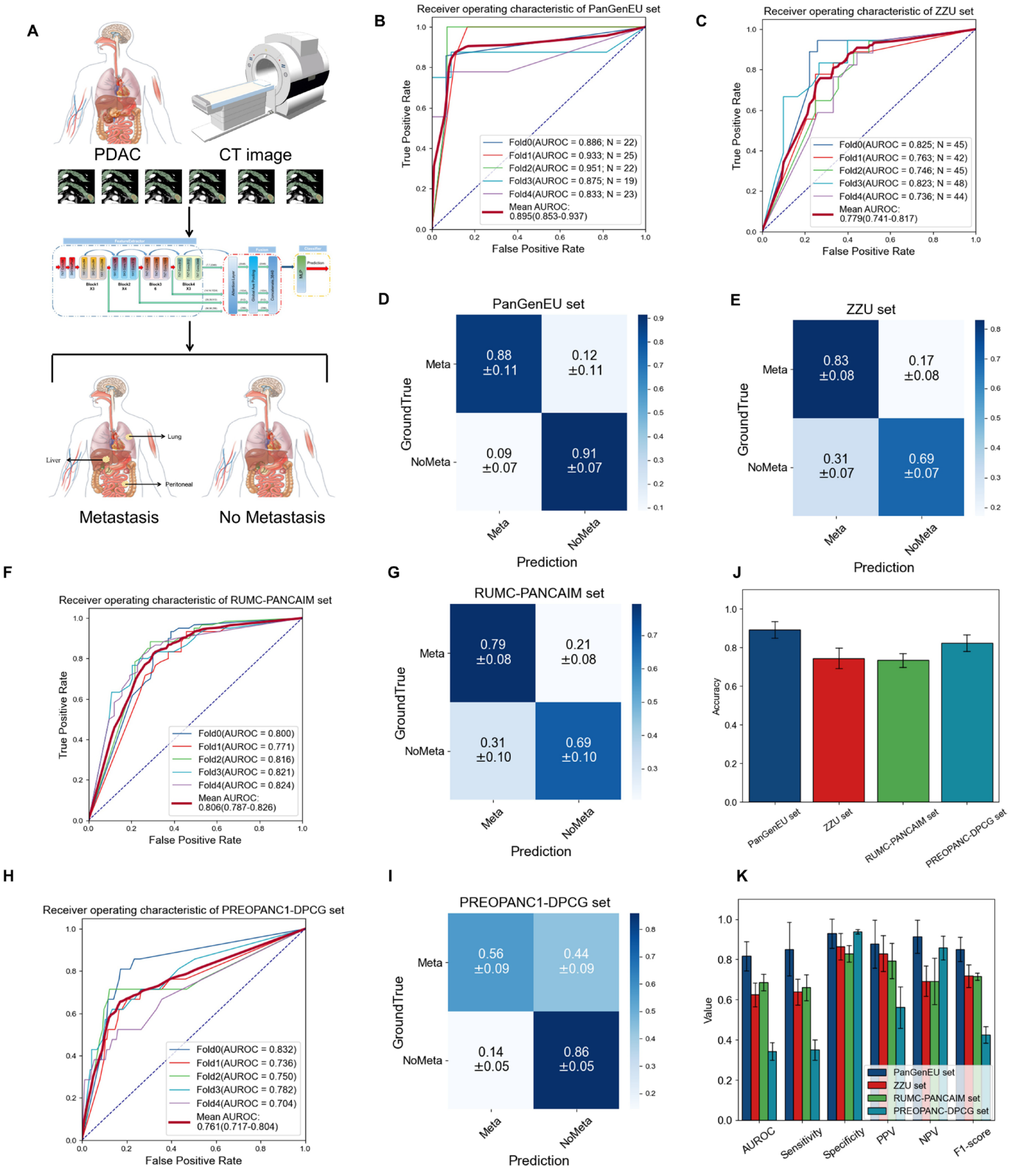

Figure 2 Performance of the PMPD model for binary classification of presence/absence of metastases at the patient level. (A) Overview of the binary classification study set-up. (B, C) Receiver operating characteristic curves (AUROC) of the PMPD-model for internal test sets (PanGenEU, ZZU). (D, E) Confusion matrices presenting the predictions for internal test sets (PanGenEU, ZZU). (F, G) AUROC and confusion matrix for the external RUMC-PANCAIM test set. (H, I) AUROC and confusion matrix for the external PREOPANC-DPCG validation set. (J, K) Distribution of the model's accuracy and the other performance matrices in the internal test sets (PanGenEU, ZZU) and the external validation sets (RUMC-PANCAIM, PREOPANC-DPCG). AUROC, area under the receiver operating characteristic curve; DPCG, Dutch Pancreatic Cancer Group; NPV, negative predictive value; PDAC, pancreatic ductal adenocarcinoma; PMPD, Pancreatic tumour Metastasis Prediction Deep learning; PPV, positive predictive value; RUMC, Radboud University Medical Center; ZZU, The First Affiliated Hospital of Zhengzhou University.

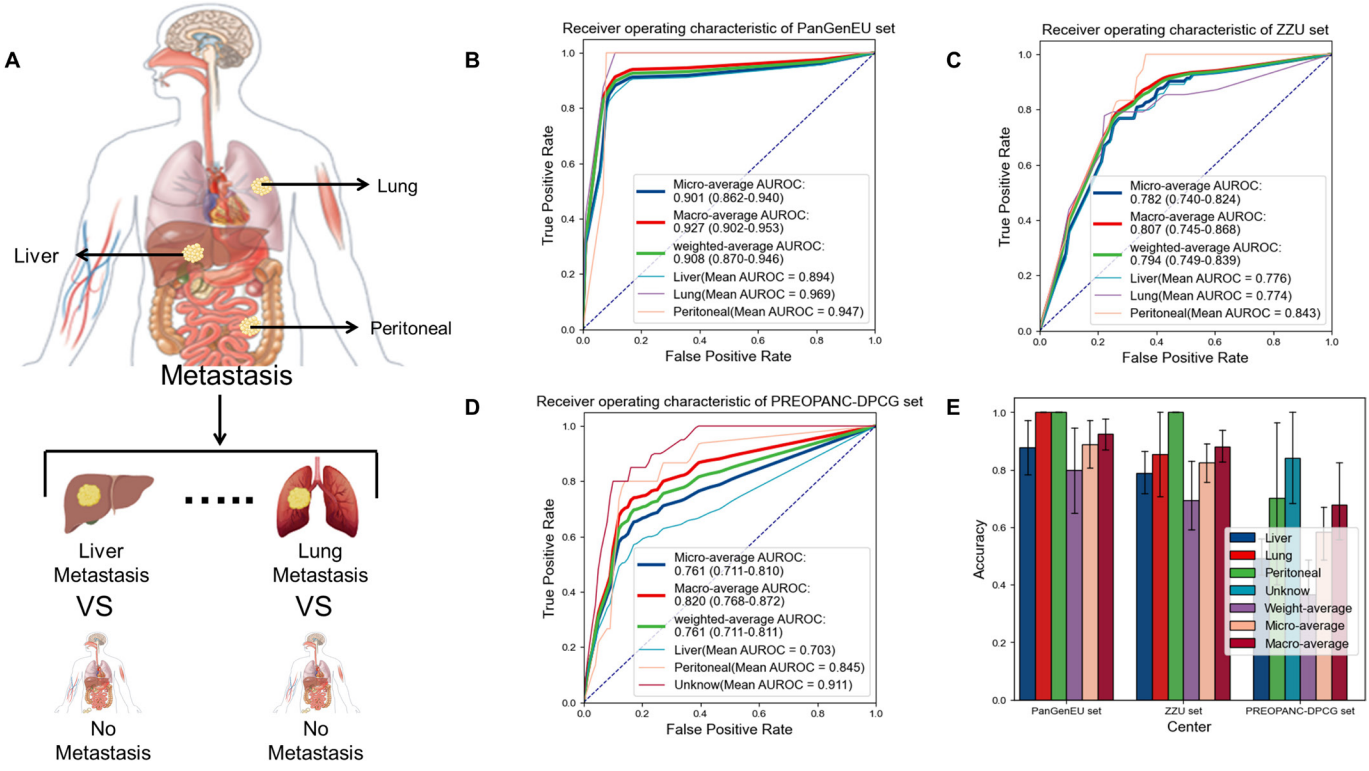

Figure 3 Performance of the PMPD-model for multinomial classification according to the metastatic sites. (A) Overview of the multinomial classification study set-up. (B, C and D) AUROC of the PMPD-model according to the metastasis sites in the internal test sets (PanGenEU, ZZU) and external validation set (PREOPANC-DPCG). (E) Distribution of the model's accuracy according to the metastasis sites. AUROC, area under the receiver operating characteristic curve; DPCG, Dutch Pancreatic Cancer Group; PMPD, Pancreatic tumour Metastasis Prediction Deep learning; ZZU, The First Affiliated Hospital of Zhengzhou University.

setting as previously associated with disease-free survival and overall survival outcomes.[26] Kaplan-Meier analysis revealed a significant difference between the high and low MRS groups (log-rank test p=2.5e−12). Notably, the MRS variable exhibited a higher HR of 2.77 (95% CI 1.99 to 3.86, p=1.59e−09) compared with the Resectability status based on univariate Cox regression (figure 4B). These findings underscore the potential of the PMPD model to provide more precise prognostic information beyond the Resectability status. The distribution of the two MRS groups according to the Resectability status is shown in online supplemental figure 5A. Kaplan-Meier curves for the MRS groups stratified by the Resectability status are displayed in online supplemental figure 5B,E. We observed that the high-MRS group patients always had a significantly worse prognosis than the low-MRS group for the Borderline Resectable and Locally Advanced of Resectability status, but not for the Resectable or metastasis.

Subsequently, we conducted comparative and combinatory analyses of the MRS and CA19-9 levels. Kaplan-Meier curves revealed a more discerning stratification capability of the MRS, outperforming the discriminatory potential of the CA19-9 levels (figure 4C). Furthermore, we explored the clinical applicability of the MRS by devising distinct patient subgroups based on MRS and CA19-9 values together. Specifically, individuals with high MRS and high CA19-9 were grouped into the high-risk group, while those with low MRS and low CA19-9 were grouped into the low-risk group. Patients falling outside these categories were designated as belonging to the mid-risk group. Remarkably, patients categorised as high-risk and mid-risk exhibited significantly worse survival outcomes compared with those classified as low-risk (HR=2.75, 95% CI 1.94 to 3.88, p=1.22e−08; and HR=1.70, 95% CI 1.26 to 2.29, p=5.28e−06), respectively (figure 4D).

Next, we conducted an in-depth examination of the MRS prognostic performance compared with the Resectability status and CA19-9 biomarker levels. In univariate Cox regression analyses, Locally Advanced and Metastasis of the Resectability status, CA19-9 values and MRS were statistically significant, with MRS having the highest HR=2.98 (95% CI 2.01 to 4.43, p=6.6e−06) (figure 4E). When including these three factors in a multivariate Cox regression, CA19-9 and MRS remained statistically significant, with MRS showing a higher HR than CA19-9 (HR=2.00 95% CI 1.21 to 3.32, p=0.000677 vs HR=1.35 (95% CI 1.03 to 1.77, p=0.0305) and the Resectability status (Metastasis, HR=1.69, 95% CI 1.10 to 2.58, p=0.01545 and Locally Advanced, HR=1.70 (95% CI 1.17 to 2.60, p=0.0135) (figure 4F). Moreover, Harrell's C-index of multivariate Cox regression building on MRS, CA19-9 and the Resectability status for overall survival yielded a value of 0.632 (figure 4G), which is higher than the individual variables, as well as for the multivariate Cox regression only, including CA19-9 and the Resectability status.

MRS predicts the metastasis development after treatment

Next, we assessed the potential utility of MRS in predicting developed metastases. We analysed 117 patients from the PanGenEU and PREOPANC-DPCG sets to achieve this. All patients were characterised as having non-metastatic disease at the time of treatment, but subsequently developed metastases during follow-up. We stratified the patients into three groups based on the timing of the development of metastasis: <3

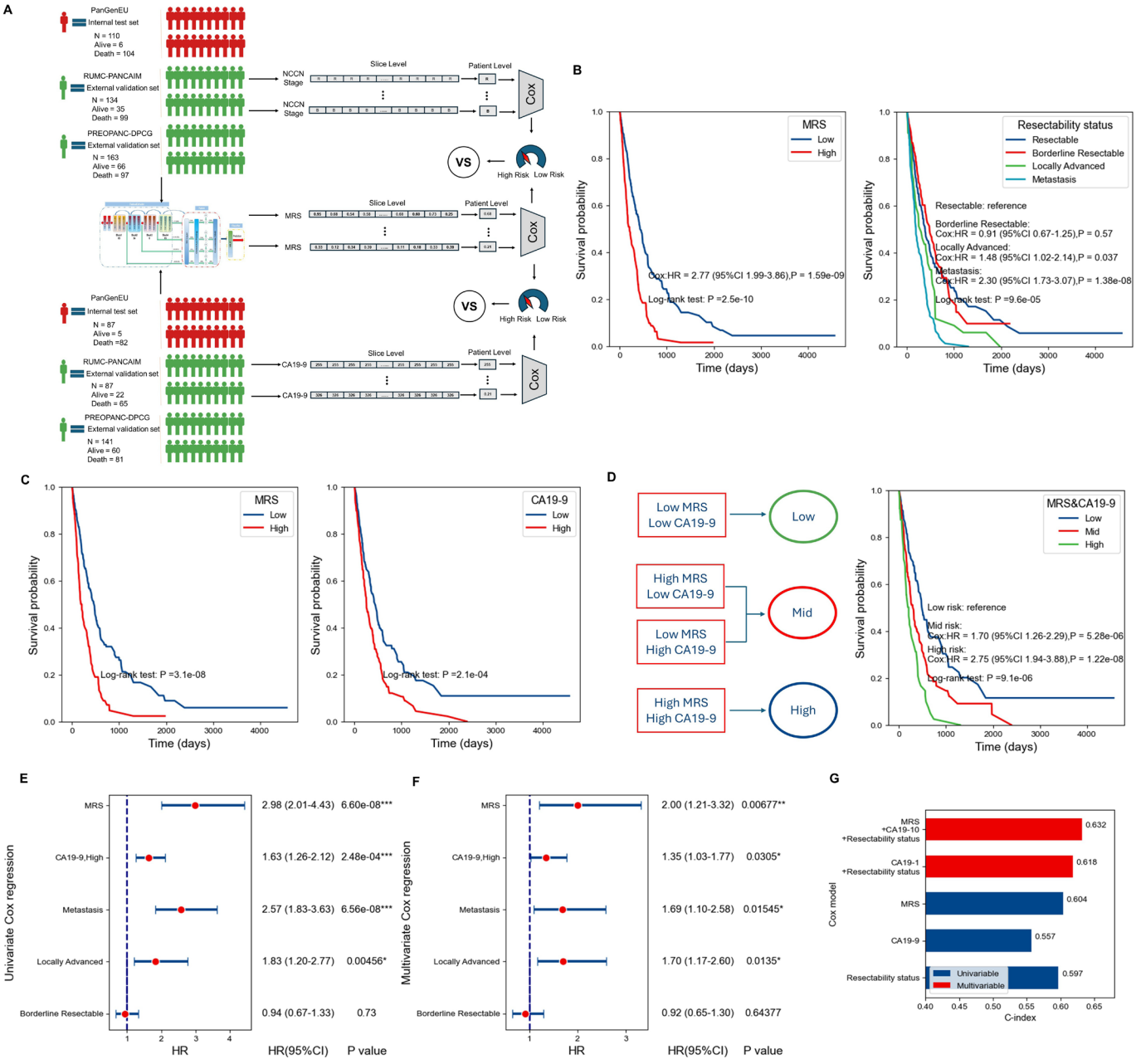

Figure 4 The prognostic ability of the Pancreatic tumour Metastasis Prediction Deep learning-model was assessed and compared with those of the Resectability status and the CA19-9 biomarker. (A) Design of prognostic value assessment of the model based on PanGenEU, DPCG and RUMC-PANCAIM sets. Following model processing, each slice yielded a metastasis risk score, which was then averaged across all slices to compute each patient's average metastasis risk score. Subsequently, the Cox regression analysis was conducted to compare the model's prognostic performance with that of the Resectability status. The same pipeline was performed to compare with CA19-9 biomarker in PanGenEU and DPCG sets. (B) Kaplan-Meier and ROC curves for the MRS and the Resectability status on 407 patients from PanGenEU, RUMC-PANCAIM and DPCG sets. Statistical significance was determined using univariate Cox regression and the log-rank test. (C) Kaplan-Meier plot and ROC curves of MRS and CA19-9 on 315 patients from PanGenEU, RUMC-PANCAIM and DPCG sets. The log-rank test was used to evaluate statistical significance. (D) Kaplan-Meier plot showing survival for the MRS subgroups stratified by CA19-9 levels. Statistical significance was determined using univariate Cox regression and the log-rank test. (E) Univariate Cox regression, (F) multivariate Cox regression and (G) C-index for the same subset of 315 patients, providing insights into the prognostic capabilities of MRS, CA19-9 and the Resectability status. CA19-9, carbohydrate antigen 19-9; DPCG, Dutch Pancreatic Cancer Group; MRS, Metastasis Risk Score; NCCN, National Comprehensive Cancer Network; ROC, receiver operating characteristic curve; RUMC, Radboud University Medical Center.

months, 3–6 months and >6 months (figure 5A). The relationship between these three metastasis timing groups and MRS is shown in figure 5B. The mean MRS of patients with metastasis developed <3 months was significantly higher than that of patients with metastasis 3–6 months and >6 months (<3 months vs 3–6 months: p=6.44e−03; <3 months vs >6 months: p=6.15e−05). However, there was no statistically significant difference in mean MRS between the 3–6 months and >6 months groups (p=0.796). We then constructed receiver operating characteristic curves for two comparisons: metastasis <3

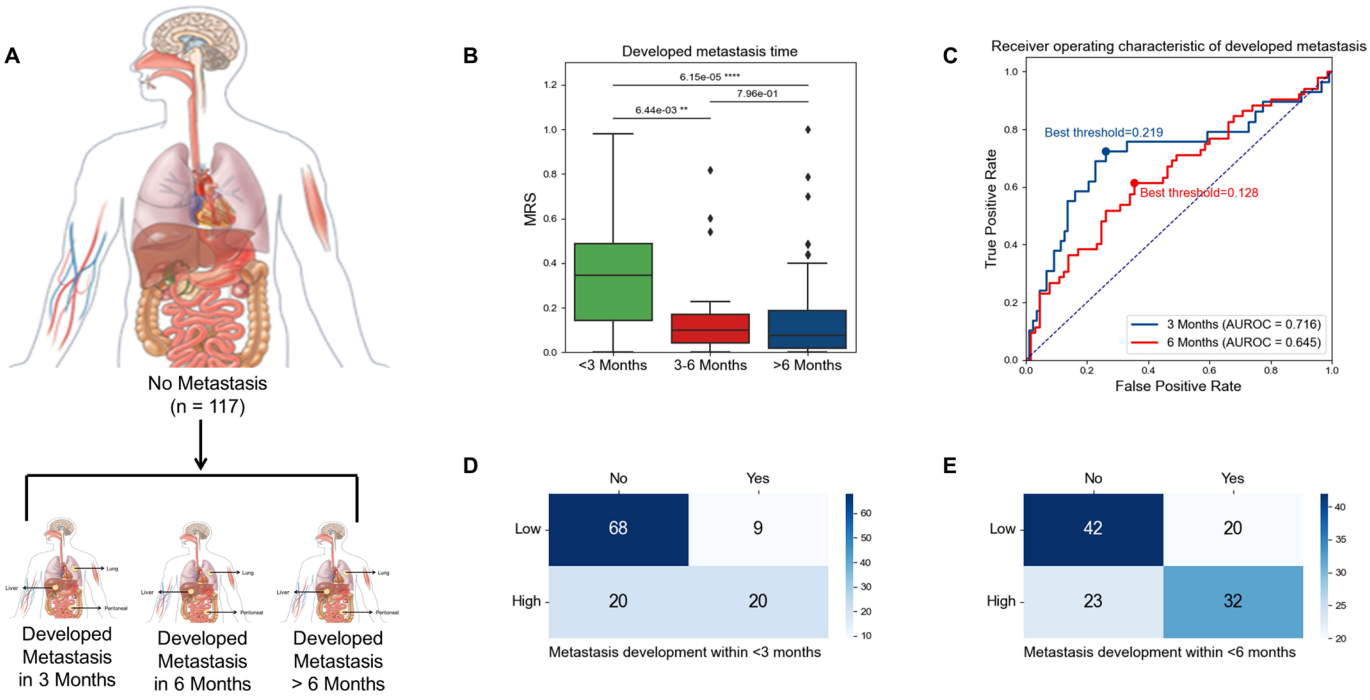

Figure 5 Evaluation of the MRS in predicting metastasis development. (A) Overview of the stratification of 117 patients based on the time to metastasis development. (B) Distribution of MRS across three metastasis timing groups: <3 months, 3–6 months and >6 months. (C) AUROCs for predicting metastasis development within <3 months versus ≥3 months and <6 months versus ≥6 months. (D, E) Confusion matrices for the high-MRS and low-MRS groups and the development of metastasis within <3 months and <6 months. AUROC, area under the receiver operating characteristic curve; MRS, Metastasis Risk Score.

months versus metastasis ≥3 months, and metastasis <6 months versus metastasis ≥6 months. These analyses resulted in area under the curves of 0.716 and 0.645, respectively (figure 5C). Using the Youden Index, we determined the maximum cut-off values for the two groups and the patients were classified into high and low MRS groups. The confusion matrices are shown in figure 5D and E.

These findings suggest that the PMPD model could potentially predict metastasis development, particularly for early metastatic events.

Visualisation for PMPD model attention characteristics

To better explore the interpretability of the PMPD model, we carried out the Grad-CAM visualisation method to mine the essential metastasis-relevant features. As depicted in figure 6, we present the activation maps of the entirely correct true positives and correct true negatives (100%: all fivefolds were accurate) on external validation cases. We found that the PMPD model accurately paid attention to both the pancreas and the tumour. Moreover, as shown in figure 6, it seemed that for non-metastatic cases, the model focused on the tumour area, following this pattern in 61.4% of the RUMC-PANCAIM set and 46.3% of the PREOPANC-DPCG set. While the model focused on smaller tumour margin areas for metastatic cases, 70% of metastasis cases in the RUMC-PANCAIM set and 66.7% of the PREOPANC-DPCG set follow this rule, which means the margins of the tumour have some features associated with metastasis.

DISCUSSION

We developed PMPD, an advanced DL algorithm for PDAC metastasis prediction that fuses abdominal CECT individual depth features from different blocks of the ResNet50 and employs a gated attention mechanism. We showed that PMPD can accurately predict the presence/absence of PDAC distant metastases both in the internal test and the external validation sets. Notably, the algorithm accurately classified 56% of the metastases in the prospective PREOPANC-DPCG set, despite the fact that they were not visualised on imaging. Furthermore, the model's performance held regardless of the metastasis location. Primary tumour size and location, patient sex and age and CT manufacturer did not affect the prediction ability of PMPD, either. We also report that the PMPD-derived MRS was the most potent independent prognostic factor, outperforming the Resectability status and CA19-9 biomarker levels. Importantly, PMPD accurately predicted 65.8% of metastases discovered through laparoscopy or during the surgical procedure that were not detected by radiographic imaging at diagnosis. Discriminating those patients at the diagnosis time could lead to more personalised treatment decisions, improving patient quality of life and saving substantial effort and economic resources. Moreover, the PMPD model could potentially predict future metastasis development, particularly for early metastatic events. To the best of our knowledge, this is the first development to adapt a CNN-based DL model in predicting clinical organ metastasis of patients with PDAC.

Previous studies implemented CT radiomics to predict lymph node metastasis in patients with PDAC by building high-performance algorithms.[17 27–29] However, robust and comprehensive prediction models for organ metastasis still need to be made available. Most patients with PDAC present with liver metastasis at first diagnosis, resulting in a poor prognosis. Zambirinis *et al* used liver radiomics of preoperative CECT scans to develop a machine-learning model with an AUROC=0.7618 to predict the presence of liver metastasis.[22] Similarly, Zhao *et al* also reported a machine learning model based on CECT achieving AUROCs between 0.71 and 0.73 in predicting liver metastases.[21]

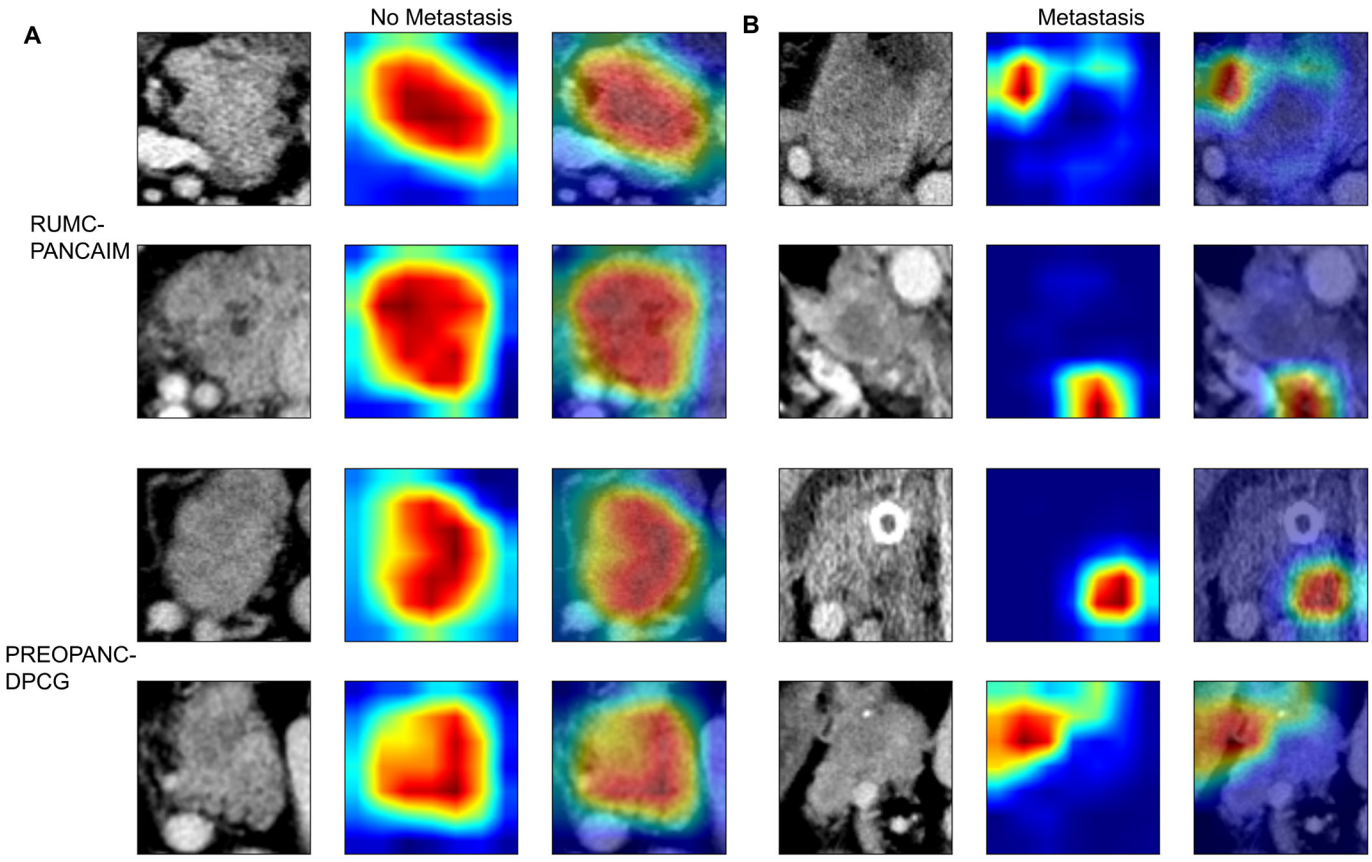

Figure 6 Examples of Grad-CAM visualisation for metastasis-relevant characteristics in the external validation sets. Subregions of focus for the model range in colour from bright blue (weak association) to dark red (strong association). Examples of true-negative (A) and true-positive (B) in RUMC-PANCAIM and PREOPANC-DPCG validation sets. DPCG, Dutch Pancreatic Cancer Group; RUMC, Radboud University Medical Center.

Compared with these previous studies, our CNN-based PMPD model achieved higher accuracy in detecting liver metastasis across the internal test datasets and the external validation dataset, and it also reached excellent prediction performance for other metastasis sites.

Furthermore, we conducted an in-depth analysis to evaluate the prognostic value of the PMPD-derived MRS and compared it against well-established prognostic factors such as the resectability status and CA19-9 biomarker levels; MRS exhibited superior prognostic performance compared with the other two prognostic factors. This observation is consistent with prior research by Zhao *et al*, as their radiomics-based model showed better predictive performance than the CA19-9 biomarker.[21] The results from the multivariable Cox regression analyses underscored the independent prognostic utility of the MRS, as evidenced by its highest HR values, which are indicative of its robust predictive capacity. Additionally, our study revealed that integrating the three factors conferred additional prognostic value to the model. Specifically, patients in the high MRS group exhibited significantly shorter overall survival than those in the low MRS group within the Borderline Resectable and Locally Advanced subgroups. Notably, the integration of MRS with CA19-9 enabled a more precise patient stratification than the CA19-9 levels alone. These results confirm MRS as the most potent independent prognostic factor, holding promise for its clinical application in guiding treatment decisions and patient management strategies.

Compared with previously reported DL approaches for medical images, PMPD has several unique characteristics. First, while previous studies have demonstrated the robustness of the fusion model in other cancer types,[30–32] in PMPD, we used a novel feature fusion method for patients with PDAC by combining feature vectors from four blocks based on the ResNet50 architecture to get holistic image information. To further boost our model's power for high-quality feature utilisation, we not only accepted Squeeze-and-Excitation Networks[29] to calculate the importance of each feature but also added learnable gating mechanism parameters to control the influence of the learnt blocks on the final output at the same time. Second, to enable PMPD to focus on pancreas areas, we cropped images into square subregions based on their mask and then combined standardised pancreas and tumour masks into a dual-channel image as the model input. This mask-guided attention technology highlights the pancreas and tumour areas in the convolutional training process. Third, as the peritumoural region plays an essential role in identifying lymph node metastasis in several cancer types,[33–35] we embraced the peritumoural region by adding $3\times3\times1$ pixels to expand the borders of the pancreas and the tumour to avoid the loss of margin information.

CECT images have greatly helped detect the presence/absence of PDAC organ metastases, but they face challenges in addressing drawbacks. The most prominent caveat is that a single abdominal CECT image cannot identify patients with distant metastasis outside the abdomen. In these situations, our proposed model, PMPD, could serve as a supplementary tool for radiologists to indicate the presence of PDAC metastasis. In addition to its diagnostic capabilities, PMPD could benefit clinical ancillary test reduction by decreasing the time and resources required to

confirm the diagnosis. This is particularly important in resource-limited settings where advanced medical imaging techniques, such as PET-CT, may not be readily available. Furthermore, PMPD can impel clinicians to advance the diagnostic workflow when the model generates metastatic predictions that conflict with the clinicians' assessment. Importantly, the PMPD model is intended to operate as a second-reader system, assisting rather than replacing radiologists. Additionally, PMPD could guide patient staging and therapeutic option decisions by providing clinicians with more accurate information about the presence and extent of metastases.

This study has several limitations that must be acknowledged. Unfortunately, there is no real 'gold standard' test to identify metastases and micrometastasis, except for autopsy, which cannot be applied in clinical practice. Therefore, we relied on the reference standard based on information reported from all clinical charts. Second, this study uses a manual checking and revision approach of the segmentations due to the insufficient performance of automatic tumour segmentation, which is labour-intensive and potentially subjective. While the most robust segmentation model currently available is nnUnet,[24] an algorithm that ranks higher in all segmentation tasks, including the pancreas and pancreatic cancer, the Dice coefficient for pancreatic cancer is still around 0.5. Therefore, future research should focus on developing more powerful segmentation methods. Third, the performance of the PREOPANC-DPCG set was slightly lower than the other sets, especially when focusing on sensitivity, F1-score and AUPRC. The first explanation is that, unlike the other datasets where metastases were more apparent on radiological imaging, the PREOPANC-DPCG set included metastatic cases not visible on imaging tests at the diagnosis time but discovered through laparoscopy or surgery afterwards. Predicting these subtle lesions is more challenging, leading to increased false negatives and, thus, a lower sensitivity. Another potential reason is the imbalanced sample size, with only 21 metastatic cases compared with 162 non-metastatic cases. Despite these challenges, the model in PREOPANC-DPCG set still achieved an AUROC of 0.761, supporting the overall high performance of PMPD. There is a further need for evaluation using datasets with prevalence rates and classifications that align closely with routine clinical practice settings. Fourth, the model's performance on the PanGenEU dataset was higher than on other datasets, which may suggest overfitting. This may be because this dataset exhibited more consistent imaging quality and annotation standards than the others. For instance, the CT protocols and scanner settings—most CT scanner platforms in PanGenEU were Philips or Siemens—supported this consistency. Finally, our study proves that the MRS performs better than the Resectability status and CA19-9. However, Harrell's C-index of the multivariate Cox regression model integrating MRS, CA19-9 and the Resectability status was 0.632, indicating a moderate level of predictive accuracy. This may be attributed to the absence of relevant data in our models, such as the type of treatment interventions or morphological/molecular characteristics of the tumour, explaining a large proportion of the variance of overall survival.

In conclusion, we developed PMPD, a DL-based fusion model that uses venous CECT images to accurately predict the presence of metastasis in patients with PDAC. The algorithm may help reduce missed metastases in CT scans and could potentially aid in guiding treatment decisions regarding surgical intervention and chemotherapy. Implementing PMPD in a real-world, real-time clinical setting represents the next step in fully assessing its impact on managing patients with PDAC's care.

Author affiliations
[1]Spanish National Cancer Research Centre, Madrid, Spain
[2]Sección de Imagen Abdominal, Hospital Vall d'Hebron, Barcelona, Catalunya, Spain
[3]Radiology, Hospital Ramón y Cajal, Madrid, Spain
[4]Universitair Medisch Centrum Sint Radboud, Nijmegen, Netherlands
[5]Genetic and Molecular Epidemiology Group, Spanish National Cancer Research Center (CNIO), Madrid, Spain
[6]Biomedical Image Technologies, ETSI Telecomunicación, Universidad Politécnica de Madrid, Madrid, Spain
[7]Centro de Investigación Biomédica en Red-BBN de Bioingeniería, Biomateriales y Nanomedicina, Instituto Salud Carlos III, Madrid, Spain, Madrid, Spain
[8]The First Affiliated Hospital of Zhengzhou University, Zhengzhou, Henan, China
[9]Radiology and Nucleas Medicine, Radboud University Medical Center Nijmegen, Nijmegen, Netherlands
[10]ErasmusMC Rotterdam, NL, /, Netherlands

Collaborators PanGenEU Centres and Investigators: Spanish National Cancer Research Centre (CNIO), Madrid, Spain: Núria Malats (Principal Investigator in each centre), Francisco X Real (Principal Investigator in each centre), Evangelina López de Maturana, Paulina Gómez-Rubio, Esther Molina-Montes, Lola Alonso, Mirari Márquez, Roger Milne, Ana Alfaro, Tania Lobato, Lidia Estudillo. Verona University, Italy: Rita Lawlor (Principal Investigator in each centre), Aldo Scarpa, Stefania Beghelli. National Cancer Registry Ireland, Cork, Ireland: Linda Sharp (Principal Investigator in each centre), Damian O'Driscoll.Hospital Madrid-Norte-Sanchinarro, Madrid, Spain: Rafael Álvarez (Principal Investigator in each centre), Manuel Hidalgo, Jesús Rodríguez Pascual. Hospital Ramon y Cajal, Madrid, Spain: Alfredo Carrato (Principal Investigator in each centre), Carmen Guillén-Ponce, Mercedes Rodríguez-Garrote, Federico Longo-Muñoz, Reyes Ferreiro, Vanessa Pachón, M Ángeles Vaz. Hospital del Mar, Barcelona, Spain: Lucas Ilzarbe (Principal Investigator in each centre), Cristina Álvarez-Urturi, Xavier Bessa, Felipe Bory, Lucía Márquez, Ignasi Poves, Fernando Burdío, Luis Grande, Mar Iglesias, Javier Gimeno.Hospital Vall d'Hebron, Barcelona, Spain: Xavier Molero (Principal Investigator in each centre), Luisa Guarner, Joaquin Balcells.Technical University of Munich, Germany: Christoph Michalski (Principal Investigator in each centre), Jörg Kleeff, Bo Kong.Karolinska Institute, Stockholm, Sweden: Matthias Löhr (Principal Investigator in each centre), Jiaqui Huang, Weimin Ye, Jingru Yu. Hospital 12 de Octubre, Madrid, Spain: José Perea (Principal Investigator in each centre), Pablo Peláez. Hospital de la Santa Creu i Sant Pau, Barcelona, Spain: Antoni Farré (Principal Investigator in each centre), Josefina Mora, Marta Martín, Vicenç Artigas, Carlos Guarner, Francesc J Sancho, Mar Concepción, Teresa Ramón y Cajal. The Royal Liverpool University Hospital, UK: William Greenhalf (Principal Investigator in each centre), Eithne Costello.Queen's University Belfast, UK: Michael O'Rorke (Principal Investigator in each centre), Liam Murray, Marie Cantwell. Laboratorio de Genética Molecular, Hospital General Universitario de Elche, Spain: Víctor M Barberá (Principal Investigator in each centre), Javier Gallego. Instituto Universitario de Oncología del Principado de Asturias, Oviedo, Spain: Adonina Tardón (Principal Investigator in each centre), Luis Barneo. Hospital Clínico Universitario de Santiago de Compostela, Spain: Enrique Domínguez Muñoz (Principal Investigator in each centre), Antonio Lozano, Maria Luaces. Hospital Clínico Universitario de Salamanca, Spain: Luís Muñoz-Bellvís (Principal Investigator in each centre), J.M. Sayagués Manzano, M.L. Gutíerrrez Troncoso, A. Orfao de Matos. University of Marburg, Department of Gastroenterology, Phillips University of Marburg, Germany: Thomas Gress (Principal Investigator in each centre), Malte Buchholz, Albrecht Neesse. Queen Mary University of London, UK: Tatjana Crnogorac-Jurcevic (Principal Investigator in each centre), Hemant M Kocher, Satyajit Bhattacharya, Ajit T Abraham, Darren Ennis, Thomas Dowe, Tomasz Radon (Principal Investigator in each centre).

Contributors NX, SS and NM conceived and led the study. XM, MM-B, MS, MO, LE, JL, RF, JJH and CvE. collected and curated data. XM, MM-B, JL, RF and JJH segmented the images. NX and SS performed analyses. NX, SS and NM wrote the original draft. MJ-L and CvE reviewed and edited the manuscript. NM supervised the work and acted as guarantor.

Funding The work was partially supported by Fondo de Investigaciones Sanitarias (FIS), Instituto de Salud Carlos III, Spain (#PI11/01542, #PI0902102, #PI12/01635, #PI12/00815, #PI15/01573; #PI18/01347; #PI21/00495); EU-6FP Integrated Project (#018771-MOLDIAG-PACA), EU-FP7-HEALTH (#259737-CANCERALIA, #256974-EPC-TMNet), H2020 (#101016851-PANCAIM). NX is awarded a PhD contract by the Chinese Scholarship Council (CSC No. 2021070040023). The funders had no role in study design, data collection and analysis, publication decision or manuscript preparation. The authors are grateful for the contributions of Tania Chadha and Benito Farina in managing preliminary images and models for this study.

Competing interests None declared.

Patient and public involvement Patients and/or the public were not involved in the design, or conduct, or reporting, or dissemination plans of this research.

Patient consent for publication Consent obtained directly from patient(s).

Ethics approval The institutional review board of the participating centres approved this study: Comité de Ética de la Investigación, Instituto de Salud Carlos III, Madrid, Spain (CEI PI 26_2025-v7_V2027-V2); Medisch Ethische ToetsingsCommissie, Erasmus MC, Rotterdam, The Netherlands (MEC-2012-249 and EudraCT-2012-003181-40); CMO Regio Arnhem-Nijmegen, The Netherlands (NL60473.091.17); The Ethics Committee of Scientific Research and Clinical Trial of The First Affiliated Hospital of Zhengzhou University (2024-KY-1774-003). Participants gave informed consent to participate in the study before taking part.

Provenance and peer review Not commissioned; externally peer reviewed.

Data availability statement Data are available upon reasonable request. Data may be obtained from a third party and are not publicly available.

ORCID iDs
Megan Schuurmans https://orcid.org/0000-0002-4939-6187
Lidia Estudillo https://orcid.org/0000-0003-3891-3713
Nuria Malats https://orcid.org/0000-0003-2538-3784

REFERENCES

1 De Dosso S, Siebenhüner AR, Winder T, *et al*. Treatment landscape of metastatic pancreatic cancer. *Cancer Treat Rev* 2021;96:102180.
2 Sohal DPS, Kennedy EB, Khorana A, *et al*. Metastatic Pancreatic Cancer: ASCO Clinical Practice Guideline Update. *J Clin Oncol* 2018;36:2545–56.
3 Bai X, Wu L, Dai J, *et al*. Rim Enhancement and Peripancreatic Fat Stranding in Preoperative MDCT as Predictors for Occult Metastasis in PDAC Patients. *Acad Radiol* 2023;30:2954–61.
4 Tsurusaki M, Numoto I, Oda T, *et al*. n.d. Assessment of Liver Metastases Using CT and MRI Scans in Patients with Pancreatic Ductal Adenocarcinoma: Effects of Observer Experience on Diagnostic Accuracy. *Cancers (Basel)*12:1455.
5 Gao J, Bai Y, Miao F, *et al*. Prediction of synchronous distant metastasis of primary pancreatic ductal adenocarcinoma using the radiomics features derived from ^{18}F-FDG PET and MRI. *Clin Radiol* 2023;78:746–54.
6 Arnone A, Laudicella R, Caobelli F, *et al*. Clinical Impact of ^{18}F-FDG PET/CT in the Diagnostic Workup of Pancreatic Ductal Adenocarcinoma: A Systematic Review. *Diagnostics (Basel)* 2020;10:1042.
7 Ducreux M, Cuhna AS, Caramella C, *et al*. Cancer of the pancreas: ESMO Clinical Practice Guidelines for diagnosis, treatment and follow-up. *Ann Oncol* 2015;26 Suppl 5:v56–68.
8 Tempero MA, Al-Hawary MM. NCCN Clinical Practice Guidelines in Oncology (NCCN Guidelines) - Pancreatic Adenocarcinoma. *Practice Guidelines* 2020.
9 Kleppe A, Skrede O-J, De Raedt S, *et al*. Designing deep learning studies in cancer diagnostics. *Nat Rev Cancer* 2021;21:199–211.
10 Schuurmans M, Alves N, Vendittelli P, *et al*. Setting the Research Agenda for Clinical Artificial Intelligence in Pancreatic Adenocarcinoma Imaging. *Cancers (Basel)* 2022;14:3498.
11 Si K, Xue Y, Yu X, *et al*. Fully end-to-end deep-learning-based diagnosis of pancreatic tumors. *Theranostics* 2021;11:1982–90.
12 Liu K-L, Wu T, Chen P-T, *et al*. Deep learning to distinguish pancreatic cancer tissue from non-cancerous pancreatic tissue: a retrospective study with cross-racial external validation. *Lancet Digit Health* 2020;2:e303–13.
13 Gregucci F, Fiorentino A, Mazzola R, *et al*. Radiomic analysis to predict local response in locally advanced pancreatic cancer treated with stereotactic body radiation therapy. *Radiol Med* 2022;127:100–7.
14 Hsu T-MH, Schawkat K, Berkowitz SJ, *et al*. Artificial intelligence to assess body composition on routine abdominal CT scans and predict mortality in pancreatic cancer– A recipe for your local application. *Eur J Radiol* 2021;142:109834.
15 He M, Chen X, Wels M, *et al*. Computed Tomography-based Radiomics Evaluation of Postoperative Local Recurrence of Pancreatic Ductal Adenocarcinoma. *Acad Radiol* 2023;30:680–8.
16 Zhang Y, Lobo-Mueller EM, Karanicolas P, *et al*. Improving prognostic performance in resectable pancreatic ductal adenocarcinoma using radiomics and deep learning features fusion in CT images. *Sci Rep* 2021;11:1378.
17 An C, Li D, Li S, *et al*. Deep learning radiomics of dual-energy computed tomography for predicting lymph node metastases of pancreatic ductal adenocarcinoma. *Eur J Nucl Med Mol Imaging* 2022;49:1187–99.
18 Bian Y, Zheng Z, Fang X, *et al*. Artificial Intelligence to Predict Lymph Node Metastasis at CT in Pancreatic Ductal Adenocarcinoma. *Radiology* 2023;306:160–9.
19 Fu N, Fu W, Chen H, *et al*. A deep-learning radiomics-based lymph node metastasis predictive model for pancreatic cancer: a diagnostic study. *Int J Surg* 2023;109:2196–203.
20 Chen X, Wang W, Jiang Y, *et al*. A dual-transformation with contrastive learning framework for lymph node metastasis prediction in pancreatic cancer. *Med Image Anal* 2023;85:102753.
21 Zhao B, Xia C, Xia T, *et al*. Development of a radiomics-based model to predict occult liver metastases of pancreatic ductal adenocarcinoma: a multicenter study. *Int J Surg* 2024;110:740–9.
22 Zambirinis CP, Midya A, Chakraborty J, *et al*. Recurrence After Resection of Pancreatic Cancer: Can Radiomics Predict Patients at Greatest Risk of Liver Metastasis? *Ann Surg Oncol* 2022;29:4962–74.
23 Shi S, Lin C, Zhou J, *et al*. Development and validation of a deep learning radiomics model with clinical-radiological characteristics for the identification of occult peritoneal metastases in patients with pancreatic ductal adenocarcinoma. *Int J Surg* 2024;110:2669–78.
24 Isensee F, Jaeger PF, Kohl SAA, *et al*. nnU-Net: a self-configuring method for deep learning-based biomedical image segmentation. *Nat Methods* 2021;18:203–11.
25 Selvaraju RR, Cogswell M, Das A, *et al*. Grad-cam: visual explanations from deep networks via gradient-based localization. 2017 IEEE International Conference on Computer Vision (ICCV); Venice, 2016
26 Anger F, Lock JF, Klein I, *et al*. Does Concurrent Cholestasis Alter the Prognostic Value of Preoperatively Elevated CA19-9 Serum Levels in Patients with Pancreatic Head Adenocarcinoma? *Ann Surg Oncol* 2022;29:8523–33.
27 Liang X, Cai W, Liu X, *et al*. A radiomics model that predicts lymph node status in pancreatic cancer to guide clinical decision making: A retrospective study. *J Cancer* 2021;12:6050–7.
28 Li K, Yao Q, Xiao J, *et al*. Contrast-enhanced CT radiomics for predicting lymph node metastasis in pancreatic ductal adenocarcinoma: a pilot study. *Cancer Imaging* 2020;20:12.
29 Hu J, Shen L, Albanie S. Squeeze-and-excitation networks. 2018 IE.EE/CVF Conference on Computer Vision and Pattern Recognition; 2017:7132–41.
30 Abdar M, Salari S, Qahremani S, *et al*. UncertaintyFuseNet: Robust uncertainty-aware hierarchical feature fusion model with Ensemble Monte Carlo Dropout for COVID-19 detection. *Inf Fusion* 2023;90:364–81.
31 Liu B, Chen C-H, Zheng P, *et al*. An Adaptive Parallel Feature Learning and Hybrid Feature Fusion-Based Deep Learning Approach for Machining Condition Monitoring. *IEEE Trans Cybern* 2022;53:7584–95.
32 Liu K, Lu N, Wu F, *et al*. Model Fusion and Multiscale Feature Learning for Fault Diagnosis of Industrial Processes. *IEEE Trans Cybern* 2022;53:6465–78.
33 Sun Q, Lin X, Zhao Y, *et al*. Deep Learning vs. Radiomics for Predicting Axillary Lymph Node Metastasis of Breast Cancer Using Ultrasound Images: Don't Forget the Peritumoral Region. *Front Oncol* 2020;10:53.
34 Wu X, Dong D, Zhang L, *et al*. Exploring the predictive value of additional peritumoral regions based on deep learning and radiomics: A multicenter study. *Med Phys* 2021;48:2374–85.
35 Wu Q, Wang S, Zhang S, *et al*. Development of a Deep Learning Model to Identify Lymph Node Metastasis on Magnetic Resonance Imaging in Patients With Cervical Cancer. *JAMA Netw Open* 2020;3:e2011625.